

## NUMERICAL SIMULATION OF DISLOCATION DYNAMICS – THE STRESS FIELD EVALUATION THRESHOLD\*

VOJTĚCH MINÁRIK<sup>1</sup>, JAN KRATOCHVÍL<sup>2</sup>, MICHAL BENEŠ<sup>1</sup>

**Abstract.** The aim of this contribution is to present the current state of our research in the field of numerical simulation of dislocation motion in crystalline materials. The simulation is based on recent theory treating dislocation curves and dipolar loops interacting by means of forces of elastic nature and hindered by the lattice friction. The motion and interaction of a single parametrically described dislocation curve and one or more dipolar loops placed in 3D space is considered. The complexity of the stress fields of dipolar loops as well as of the dislocation curve necessitates application of advanced numerical algorithms to successfully solve the problem. The present numerical algorithm is based on analytical formulae for stress tensor of interaction between dislocation curve and dipolar loop, analytical interaction formulae for dipolar-to-dipolar loop interaction, parametric description of the dislocation curve (i.e. 1D description of a fully 3D problem), and the flowing finite volume method. It is showing up, that despite of using analytical formulae in the numerical algorithm, it is necessary to introduce other optimizations as distance thresholds for evaluation of these formulae.

**Key words.** dislocation dynamics, stress field, MCFL, mean-curvature flow

**AMS subject classifications.** 35K65, 68U20, 74M25, 74S10

**1. Numerical Model.** In our model of dislocation dynamics, discrete solution of the dislocation curve is represented by a moving polygon given, at any time  $t$ , by plane points  $\vec{X}_i, i = 0, \dots, M$ . The values  $\vec{X}_0$  and  $\vec{X}_M$  of the end points are prescribed in case of fixed ends of the curve, i.e. the values do not depend on time. The segments  $[\vec{X}_{i-1}, \vec{X}_i]$  are called flowing finite volumes. The evolution equation of the dislocation curve has the form of intrinsic diffusion equation [1], [2], [4]. By integrating in dual volumes and using some other straightforward steps described in [7] we get a system of ordinary differential equations for the points of the polygon:

$$B \frac{d\vec{X}_i}{dt} = \varepsilon \frac{2}{d_i + d_{i+1}} \left( \frac{\vec{X}_{i+1} - \vec{X}_i}{d_{i+1}} - \frac{\vec{X}_i - \vec{X}_{i-1}}{d_i} \right) + \frac{2}{d_i + d_{i+1}} F_i \frac{\vec{X}_{i+1}^\perp - \vec{X}_{i-1}^\perp}{2},$$

$i = 1, \dots, M - 1. \quad (1.1)$

In the above ODE system,  $d_i$  denote distances between neighbouring nodes of the dislocation curve's discretization. Obviously, we have to complete the ODE system by including differentials  $\frac{d\vec{X}_0}{dt}$  and  $\frac{d\vec{X}_M}{dt}$ . The exact form of these differentials depends on the particular model we use.

The governing equations for the motion of dipolar loops, that are allowed to move

---

\*This work was partially supported by Nečas Center for Mathematical Modeling, project LC06052 of the Ministry of Education of the Czech Republic

<sup>1</sup>Department of Mathematics, Faculty of Nuclear Sciences and Physical Engineering, Czech Technical University in Prague, Trojanova 13, 120 00 Prague 2, Czech Republic (Vojtech.Minarik@fjfi.cvut.cz, Michal.Benes@fjfi.cvut.cz).

<sup>2</sup>Department of Physics, Faculty of Civil Engineering, Czech Technical University in Prague, Thákurova 7, 166 29 Prague 6 (kratochvil@fsv.cvut.cz).

only along the x-axis, consist of another system of ODE:

$$\frac{dx^{(j)}(t)}{dt} = \frac{1}{BP} F_{x,total}^{(j)}(\vec{X}_0(t), \dots, \vec{X}_M(t), x^{(0)}(t), \dots, x^{(N)}(t)), \quad j = 1, \dots, N, \quad (1.2)$$

where  $x^{(j)}(t)$  denotes the x-axis position of the j-th dipolar loop, and  $F_{x,total}^{(j)}$  (depending on positions of the dislocation curve and all the other dipolar loops) denotes the total forces acting on the j-th dipolar loop.

The complete discrete problem consists of (1.1) and (1.2) with accompanying initial and boundary conditions. The initial conditions simply describe positions and shapes of the dislocation curve and dipolar loops at the beginning of the computation. The boundary conditions differ depending on the particular model (both mathematical and numerical) we solve. The terms  $F_i$  in (1.1) and  $F_{x,total}^{(j)}$  in (1.2) include stress fields of dipolar loops as well as the interactions among the dipolar loops, which both are very complex.

The analytical formula for the stress field generated by a single dipolar loop of type  $V_1$ ,  $V_2$ ,  $I_1$ , or  $I_2$ <sup>1</sup> is based on the formula presented by Kroupa in [3]. Due to some special arrangements of our model it reads:

$$\begin{aligned} \sigma_{xy}(x, y, z) = & -\frac{\mu hb}{2\pi(1-\nu)} \left\{ \left[ \frac{l-z}{\varrho_-} + \frac{l+z}{\varrho_+} \right] \left[ \frac{x \pm y}{(x^2 + y^2)^2} (\pm x + y - 8 \frac{x^2 y}{x^2 + y^2}) \right] \right. \\ & + \left[ \frac{l-z}{\varrho_-^3} + \frac{l+z}{\varrho_+^3} \right] \left[ \pm \nu + \frac{xy}{(x^2 + y^2)^2} (y^2 - 3x^2 \mp 4xy) \right] \\ & \left. + \left[ \frac{l-z}{\varrho_-^5} + \frac{l+z}{\varrho_+^5} \right] \left[ -\frac{3x^2 y (x \pm y)}{x^2 + y^2} \right] \right\}, \quad (1.3) \\ \varrho_- = & \sqrt{x^2 + y^2 + (l-z)^2}, \quad \varrho_+ = \sqrt{x^2 + y^2 + (l+z)^2}, \end{aligned}$$

where  $\sigma_{xy}$  stands for the xy-component of the stress field tensor,  $x, y, z$  is the relative position of the point we want to evaluate the stress in,  $\mu$  is shear modulus,  $h$  and  $l$  are the half-width and half-length of a dipolar loop,  $b$  is the Burgers vector, and  $\nu$  is the Poisson's ratio.

The interaction between two dipolar loops in stable configurations is described by analytical formulae which were presented in [5]. It depends on the combination of the types and configurations of both dipolar loops.

The first formula holds for the combinations  $V_1 - V_2$ ,  $V_1 - I_2$ ,  $I_1 - V_2$ ,  $I_1 - I_2$ ,  $V_2 - V_1$ ,  $V_2 - I_1$ ,  $I_2 - V_1$ , and  $I_2 - I_1$ :

$$\begin{aligned} F_x^{(1)} = & -\frac{\mu h^2}{\pi(1-\nu)} b' b'' \left\{ \xi_1 \frac{-8x_0^5 + 64x_0^3 y_0^2 - 24x_0 y_0^4}{(x_0^2 + y_0^2)^4} + \xi_{-1} \frac{-4x_0^5 + 32x_0^3 y_0^2 - 12x_0 y_0^4}{(x_0^2 + y_0^2)^3} \right. \\ & \left. + \xi_{-3} \left( (1-\nu)x_0 + \frac{-x_0^5 + 8x_0^3 y_0^2 - 3x_0 y_0^4}{(x_0^2 + y_0^2)^2} \right) + \xi_{-5} \left( 3x_0^3 \frac{-x_0^2 + y_0^2}{x_0^2 + y_0^2} \right) \right\}. \quad (1.4) \end{aligned}$$

For the combinations  $V_1 - V_1$ ,  $V_1 - I_1$ ,  $I_1 - V_1$ ,  $I_1 - I_1$ , there is the second formula (using the upper signs). Finally, for  $V_2 - V_2$ ,  $V_2 - I_2$ ,  $I_2 - V_2$ , and  $I_2 - I_2$ , there is

<sup>1</sup>Each dipolar loop is described by a letter and a subindex. Letters  $V$  and  $I$  stand for vacancy and interstitial dipolar loops, subindices 1 and 2 denote stable configurations as presented in [7], [6].

the third formula (with the lower signs):

$$\begin{aligned}
 F_x^{(2,3)} = & -\frac{\mu h^2}{\pi(1-\nu)} b' b'' \left\{ -4\xi_1 \frac{x_0^5 \pm 9x_0^4 y_0 - 2x_0^3 y_0^2 \mp 14x_0^2 y_0^3 - 3x_0 y_0^4 \pm y_0^5}{(x_0^2 + y_0^2)^4} \right. \\
 & + \xi_{-1} \frac{-2x_0^5 \mp 18x_0^4 y_0 + 4x_0^3 y_0^2 \pm 28x_0^2 y_0^3 + 6x_0 y_0^4 \mp 2y_0^5}{(x_0^2 + y_0^2)^3} \\
 & \left. + \xi_{-3} \left( (1+\nu)x_0 + \frac{-x_0^5 \mp 4x_0^4 y_0 \pm 8x_0^3 y_0^2 + x_0 y_0^4}{(x_0^2 + y_0^2)^2} \right) + \xi_{-5} \left( -3x_0^3 \frac{(x_0 \pm y_0)^2}{x_0^2 + y_0^2} \right) \right\}. \quad (1.5)
 \end{aligned}$$

In all three above formulae we use the following shorthand notation:

$$\begin{aligned}
 \xi_1 &= \rho_0(-2l) - 2\rho_0(0) + \rho_0(2l), & \xi_{-1} &= -\frac{1}{\rho_0(-2l)} + 2\frac{1}{\rho_0(0)} - \frac{1}{\rho_0(2l)}, \\
 \xi_{-3} &= -\frac{1}{\rho_0^3(-2l)} + 2\frac{1}{\rho_0^3(0)} - \frac{1}{\rho_0^3(2l)}, & \xi_{-5} &= -\frac{1}{\rho_0^5(-2l)} + 2\frac{1}{\rho_0^5(0)} - \frac{1}{\rho_0^5(2l)}, \\
 \rho_0(\omega) &= \rho_0(x_0, y_0, z_0, \omega) = \sqrt{x_0^2 + y_0^2 + (z_0 + \omega)^2}. \quad (1.6)
 \end{aligned}$$

**2. Stress Field Evaluation Threshold.** Having the analytical formula for the stress field  $\sigma_{xy}$  and the interaction force of a pair of dipolar loops may seem to be enough for fast computation. However, this is not true. According to the profiling results of disdyn<sup>2</sup> code for a test case having 10 dipolar loops and single dislocation curve consisting of 2000 segments, about 93% of CPU time was spent in computation of  $\sigma_{xy}$  and about 5% in computation of interactions among dipolar loops. The rest was spent in Runge-Kutta and other supplemental algorithms.

With employment of a cut-off distance for  $\sigma_{xy}$  computation, which was set to 50 nanometers<sup>3</sup>, the profiling results were much better. CPU time spent in computation of  $\sigma_{xy}$  fell down to about 60%, while the unchanged (i.e. still not using the threshold) interaction force among dipolar loops arised to 20%.

All  $\sigma_{xy}$ ,  $F_x^{(1)}$ ,  $F_x^{(2)}$ , and  $F_x^{(3)}$  are explicit formulae which therefore are fast to evaluate for a single set of parameters (comparing to the integrals in the original Kroupa formula). However, these proved to be CPU time expensive in the simulation due to the fact we need to evaluate them very often (98% of the CPU time in the above mentioned test). Obviously, the count of evaluations of each formula depends on the exact setting of the test simulation. Denote  $e_\sigma$  the count of evaluations of the stress field component  $\sigma_{xy}$  and  $e_{DL}$  the count of evaluations of the interaction between a pair of dipolar loops. Having  $M$  the number of segments of the dislocation curve and  $N$  the number of dipolar loops, for a particular time step of the Runge-Kutta method it holds:

$$e_\sigma = 4N(2M - 1), \quad (2.1)$$

$$e_{DL} = 4N(N - 1). \quad (2.2)$$

In (2.1) the constant 4 stands for substeps of the Runge-Kutta method,  $M$  segments of the dislocation curve affect the motion of  $N$  dipolar loops. Vice-versa,  $M - 1$  inner nodes of the dislocation curve are affected by the stress fields of  $N$  dipolar loops. In

<sup>2</sup>The computational program developed to implement numerical simulation of dislocation dynamics

<sup>3</sup>Justification of this choice is presented later in this section

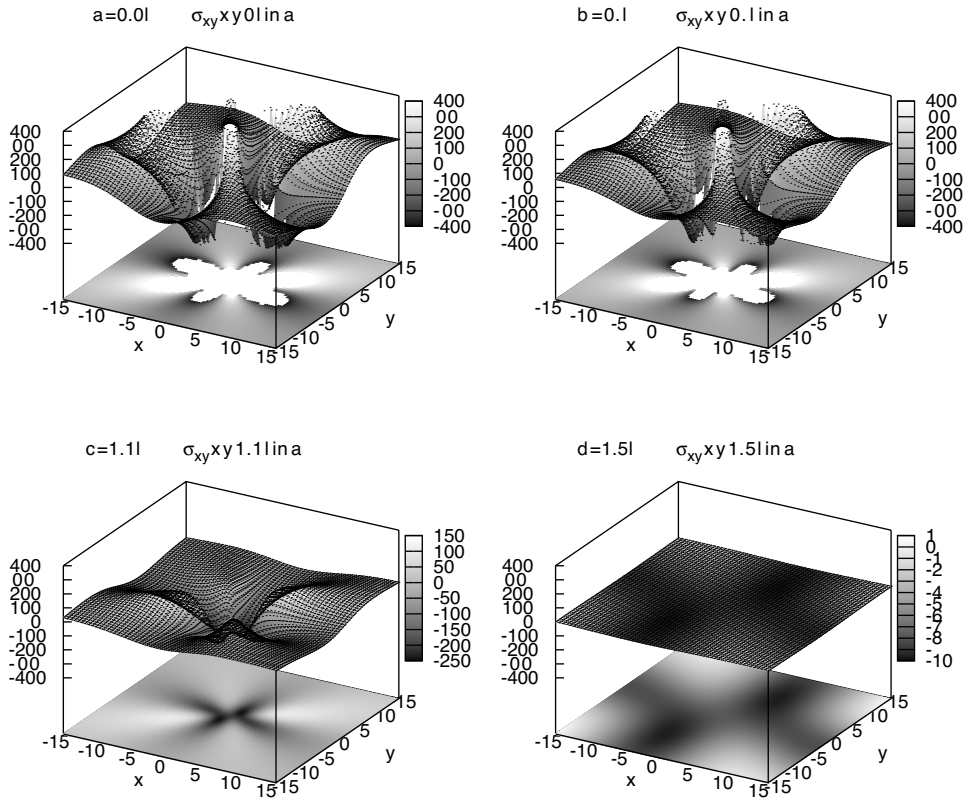


FIG. 2.1. Graphs of the stress field component  $\sigma_{xy}$  generated by a dipolar loop  $V_1$  centered in the origin of the coordinate system – several fixed values of  $z$  displayed: a)  $z = 0.0l$ , b)  $z = 0.9l$ , c)  $z = 1.1l$ , and d)  $z = 1.5l$

(2.2), for each of the  $N$  dipolar loops, there is an interaction with all other  $N - 1$  loops, the constant 4 is the number of substeps of the Runge-Kutta method as in (2.1).

Just for imagination, in the setting we profiled, a particular time step of Runge-Kutta method consists of 159960 evaluations of the stress field and 360 evaluations of interactions between a pair of dipolar loops. As we can see in (2.1) and (2.2), the increase in the number of segments  $M$  influences  $e_\sigma$  linearly. However, this cannot be said about the increase of the number of dipolar loops. For example, using  $N = 100$  instead of  $N = 10$  in the above test simulation would lead to ten times higher  $e_\sigma$  (1599600), but  $e_{DL}$  would change more dramatically from 360 to 39600. For  $N = 1000$ ,  $e_{DL}$  would grow even more to 3996000. Therefore, there were two important motivations for improving the speed of the algorithm. The first, we want to run our model with a bigger amount of dipolar loops, and the second, even in the above presented test case with small number of dipolar loops the computation was too slow.

**2.1. Optimizing the stress field evaluation.** There is a simple idea how to make the stress field evaluation faster. The stress field is evaluated many times during the algorithm, and many times it evaluates to a value which is near to zero. This

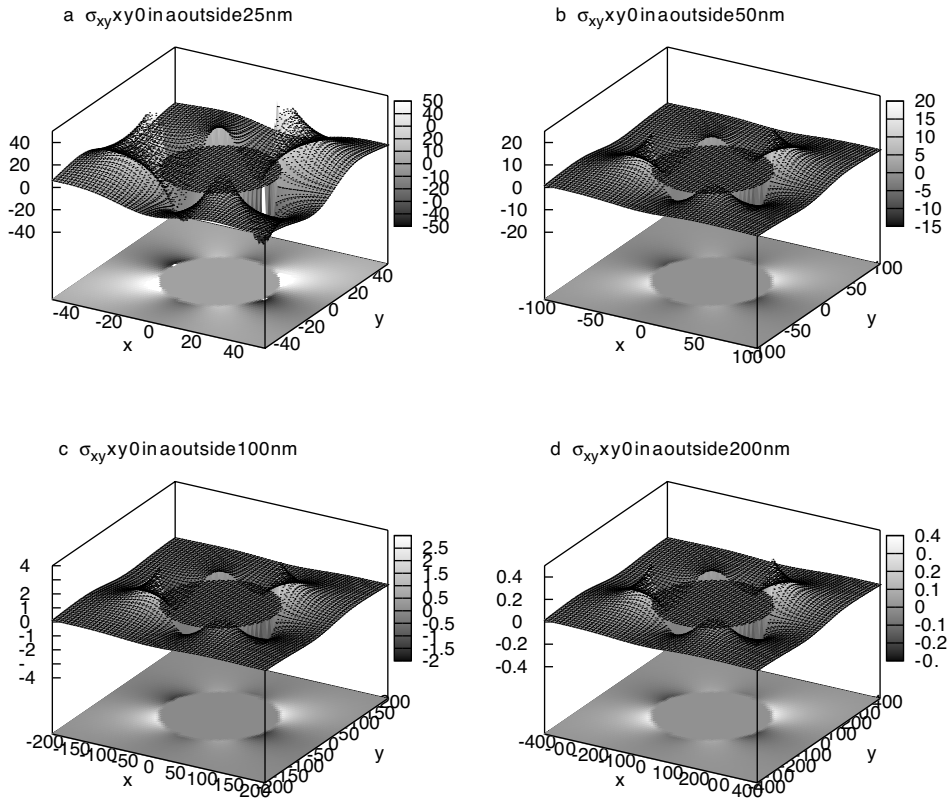


FIG. 2.2. Minimum and maximum values of the stress field beyond a circular threshold

is because of the fact that the stress field is of a short-range type and vanishes very quickly as the distance from the generating dipolar loop is growing. Thus, putting a threshold distance into the algorithm seems to be straightforward. We simply neglect the stress generated by a dipolar loop if the point, at which we want to evaluate the stress, is far enough from the dipolar loop. However, it is not an easy task to setup the threshold value properly. We have to make it small enough to speed-up the computation, but we should not make it too small as that can lead to inaccurate simulation results. Obviously, the threshold distance depends on all the parameters of the stress field formula. The rest of this section will use following setting of physical parameters which were experimentally measured for nickel crystals at room temperature [8]:  $\mu = 80$  GPa,  $\nu = 0.31$ ,  $b = 0.26$  nm,  $l = 30$  nm,  $h = 2$  nm.

Fig 2.1 shows the stress field of a dipolar loop of type  $V_1$  for several fixed values of  $z$  (in terms of multiples of dipolar loop half-length  $l$ ), while  $x$  and  $y$  coordinates are plotted in the graphs. Note here the orientation of the coordinate system – the  $z$ -axis lies whole in the gliding plane, whereas the  $y$ -axis is the distance of the center of the dipolar loop from the gliding plane. It can be seen that the stress field is changing rapidly in the closest neighbourhood of the centre of the dipolar loop generating the field, whereas it vanishes fast as the distance from the loop is growing. Next we discuss consequences of neglecting the stress field beyond some threshold distance from the

TABLE 2.1

Minimal and maximal values of the stress field outside of a circle around the centre of a dipolar loop, evaluated in planes  $z = 0$ ,  $z = l$ , and  $z = -l$ .

Threshold radius $r$	$z = 0$ nm		$z = \pm l$ nm	
	min $\sigma_{xy}$	max $\sigma_{xy}$	min $\sigma_{xy}$	max $\sigma_{xy}$
25 nm	-60 MPa	80 MPa	–	–
50 nm	-15 MPa	20 MPa	-15 MPa	15 MPa
100 nm	-2 MPa	3 MPa	-1.5 MPa	2.5 MPa
200 nm	-0.3 MPa	0.4 MPa	-0.2 MPa	0.4 MPa
300 nm	-0.08 MPa	0.12 MPa	-0.08 MPa	0.12 MPa

centre of the dipolar loop. Fig 2.2 shows the stress field outside the circles of various radiuses. To be more precise, each figure shows the stress field values outside the circle of a particular radius, whereas the values inside the circle are set to zero. This allows us to compare the minimal and maximal values available at different distances from the centre of the dipolar loop (see the color-bars on the right from the graphs). Only the plane  $z = 0$  is showed in Fig 2.2 as the absolute minimum and maximum values of stress field fall down with growing distance from this plane. Hence, the other planes are not important for the idea which follows.

Tab 2.1 shows the minimal and maximal values of the stress field beyond the threshold distance (outside the circle of radius  $r$ ) we picked from the graphs in Fig. 2.2. We can see that the stress field values beyond the 200 nm radius are at least 7 times smaller than beyond the 100 nm radius. However, the area of the interaction in the annulus between 200 nm and 300 nm radiuses is much larger than the area of the annulus between 100 nm and 200 nm radiuses. What error we commit if we neglect the stress field in the annulus bounded between radiuses  $r_0$  and  $r_1$ ? To estimate the error, we do the following. First, we assume that the maximum stress field value in the annulus is achieved in the whole annulus. Note this is a big overestimate. Second, consider the fact that the stress field of a dipolar loop interacts with segments of dislocation curve in the simulation. The force influence would be the biggest if all the curve segments would be oriented the same (i.e. the dislocation curve would be a straight line). However, this would not fit into the annulus as the typical length of the dislocation curve is several micrometres. Therefore, assuming a circular dislocation curve inside the annulus, and ignoring the real orientations of the segments, we commit another two overestimates. The first one is that the segments are obviously not oriented the same; the second one is that though such a circular curve is rather long, it is surely not real. Nevertheless, assume a circular dislocation curve with the center of the circle identical with the center of the annulus. Then the length of the curve would be  $2\pi(r_0 + r_1)/2$ .

Using all the above information, we can evaluate upper estimates of the total force (generated by a dipolar loop) acting on a dislocation curve in the annulus, and, vice versa, the total force acting on that dipolar loop (as a reaction of the dislocation curve). We refer to [5] for the formula  $F_x^{c(i)}$  of the interaction force between  $i^{th}$  dipolar loop and the whole dislocation curve:

$$F_x^{c(i)} = \int_X \sigma_{xy}^{(i)} b n_x dX . \quad (2.3)$$

Denote  $L$  the length of the dislocation curve. Let  $n_x = 1$  (assuming the same ori-

TABLE 2.2  
Neglected force estimation in several annuli between  $r_0$  and  $r_1$

$r_0$	$r_1$	$L$ – Dislocation curve length	$F_{est}$ Force estimate	$F_{est}/L$
25 nm	50 nm	250 nm	5.2 nN	0.0208
50 nm	100 nm	450 nm	2.5 nN	0.00556
100 nm	200 nm	1000 nm	0.78 nN	0.00078

TABLE 2.3  
Hausdorff distance of dislocation curves measured at  $t = 15.0004$  for several values of threshold

Threshold	25 nm	50 nm	75 nm	100 nm	off
25 nm	–	1.32	1.31	1.31	1.87
50 nm	1.32	–	0.47	0.57	1.56
75 nm	1.31	0.47	–	0.51	1.53
100 nm	1.31	0.57	0.51	–	1.09
off	1.87	1.56	1.53	1.09	–

entation of all curve segments). The force estimate  $F_{est}$  (which serves as a quantity identifying fraction of interaction force which is to be neglected) is based on (2.3) and is summarized in Tab 2.2 – together with the value per the unit length of the dislocation curve  $F_{est}/L$ :

$$F_{est} = Lb \max \sigma_{xy} . \quad (2.4)$$

Table 2.2 suggests that the threshold distance of 50 nm can be used. This choice can be supported by Tab 2.3 as well. Here the simulation for threshold values 25, 50, 75, and 100 nm is compared to the simulation without any distance restriction. The evolution ends at time  $t = 15.0004$  at which we evaluated the Hausdorff distances between the dislocation curves. In the last column of Tab 2.3, the convergence for growing threshold value is observed. Between the pairs 50-75, 50-100, and 75-100 the distances are almost the same and smaller than for the pairs 25-50, 25-75, and 25-100. This justifies the threshold choice between 25 and 50 nm. We choose the threshold 50 nm in order to avoid the so-called bleeding edge which could make the simulation algorithm unstable or inaccurate.

**3. Numerical results.** We applied the above presented threshold for evaluating the interaction between a particular segment of a dislocation curve and a single dipolar loop into the numerical algorithm and present here some results. In Fig. 3.1 there are several time levels of a simulation consisting of a single dislocation curve (initial length  $1.2 \mu\text{m}$ ), 5 vacancy dipolar loops  $V_1$  with  $y$ -coordinate equal to  $-10, 10$  (twice),  $15$  and  $20$  nm, and 5 vacancy dipolar loops  $V_2$  with  $y$ -coordinate equal to  $-10, 10$  (twice),  $-15$  and  $-20$  nm. The left-hand side of figure contains 3D plots with position of the curve and loops, whereas the righthand side contains 2D projection of their positions onto the gliding plane of the dislocation curve. Each time four closely following time levels are brought together into one graph to provide better understanding of the dynamics at the given time moments.

The simulation has been performed in order to study the clustering phenomenon which is initially observed at  $t = 46.004$ . Then the cluster does not substantially change its shape in the following time levels. In general, the cluster formation highly

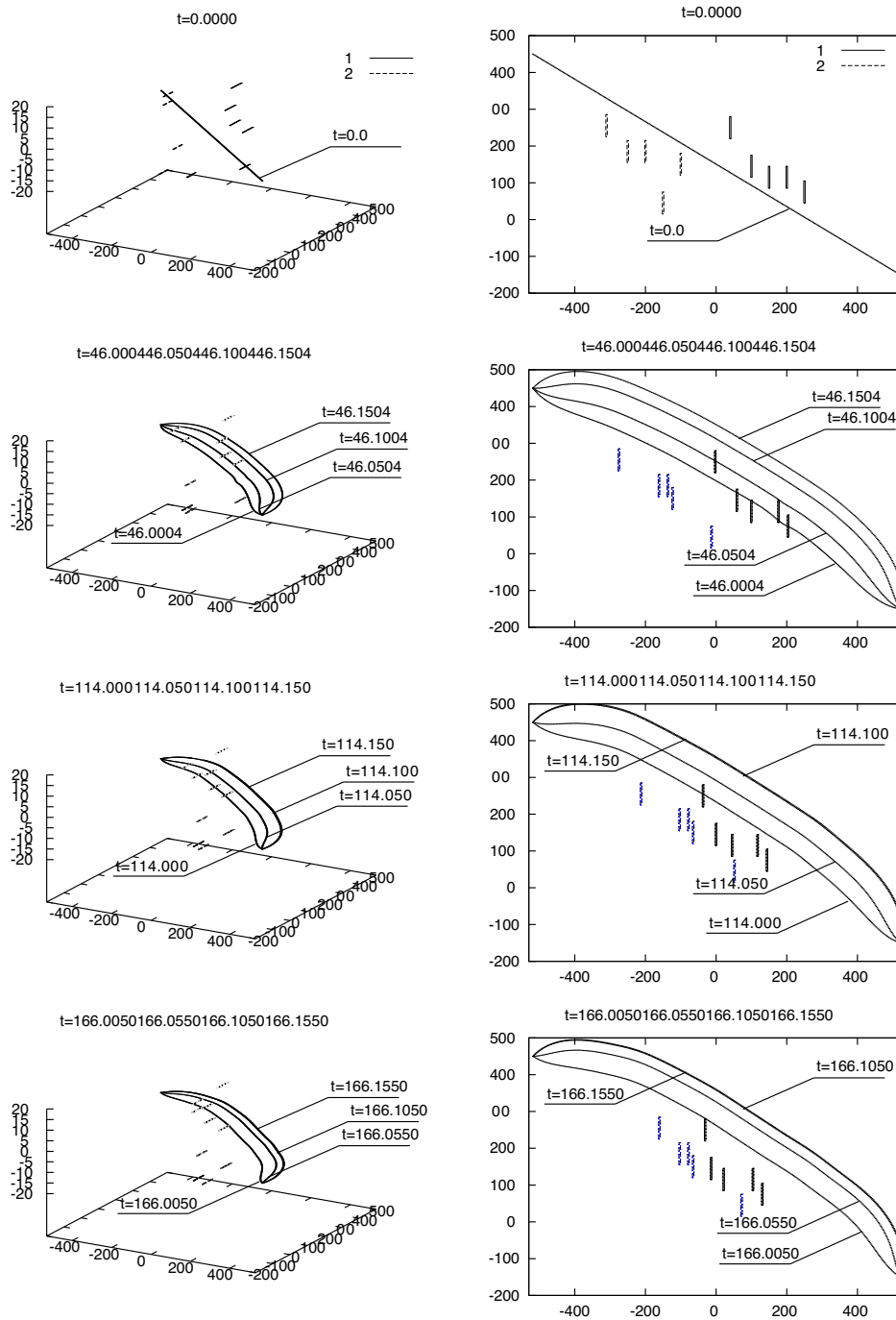


FIG. 3.1. TEST 1 – Clustering phenomenon. Interaction dynamics between a dislocation and 10 dipolar loops of of  $V_1$  and  $V_2$  type. Graphs on left show spatial positions of interacting objects, graphs on right show projection of the positions onto the glide plane.

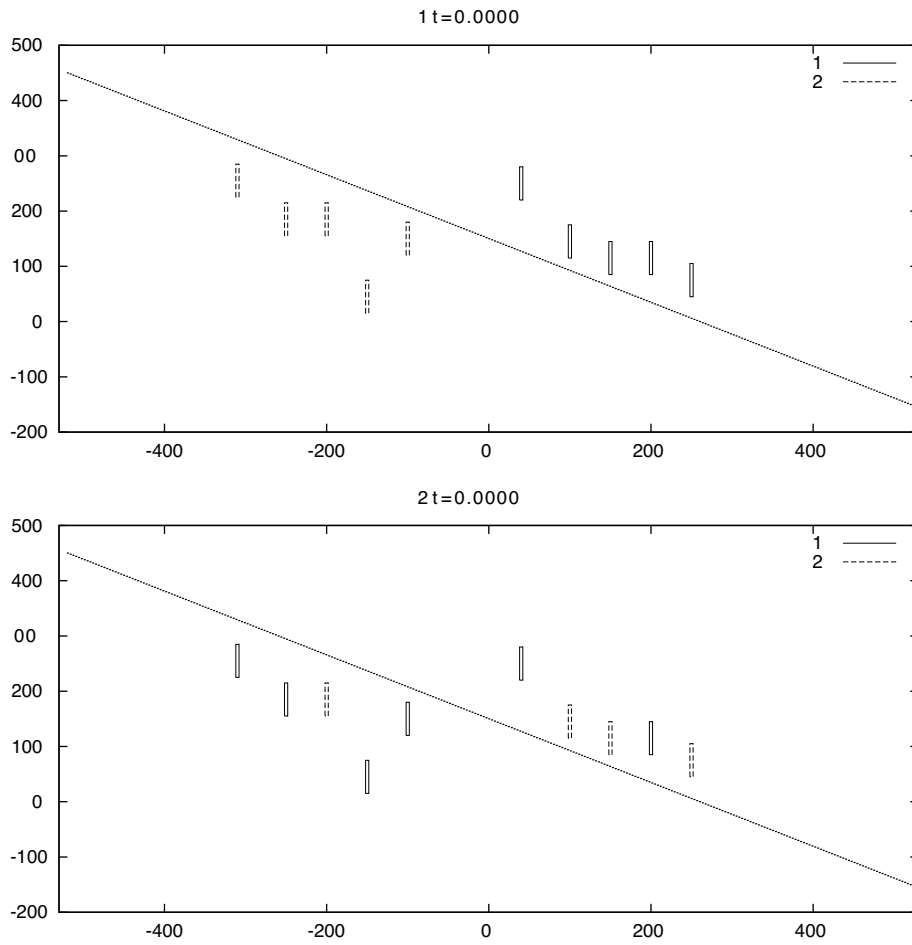


FIG. 3.2. Initial conditions of simulations *TEST 1* and *TEST 2* – single dislocation and 10 dipolar loops.

depends on the initial conditions where the initial positions of the dipolar loops play important role. Additionally, a change in types of dipolar loops (using the same initial positions) produces a different result in terms of mutual positions. This fact is illustrated in Fig. 3.2 and 3.3. Fig. 3.2 shows the two initial setups – in the second one we changed 4  $V_1$  dipolar loops to  $V_2$  and 4  $V_2$  to  $V_1$ . Fig. 3.3 shows the simulation results close to  $t = 166.005$  for both setups. As we can see, the positions of dipolar loop substantially differ in both simulations – clustering phenomenon from the *TEST 1* is replaced by a wide opening in which the dipolar loops move outwards in the *TEST 2*.

**Acknowledgements.** The authors were partly supported by the Jindřich Nečas Center for Mathematical Modeling, project LC06052 of the Ministry of Education of the Czech Republic.

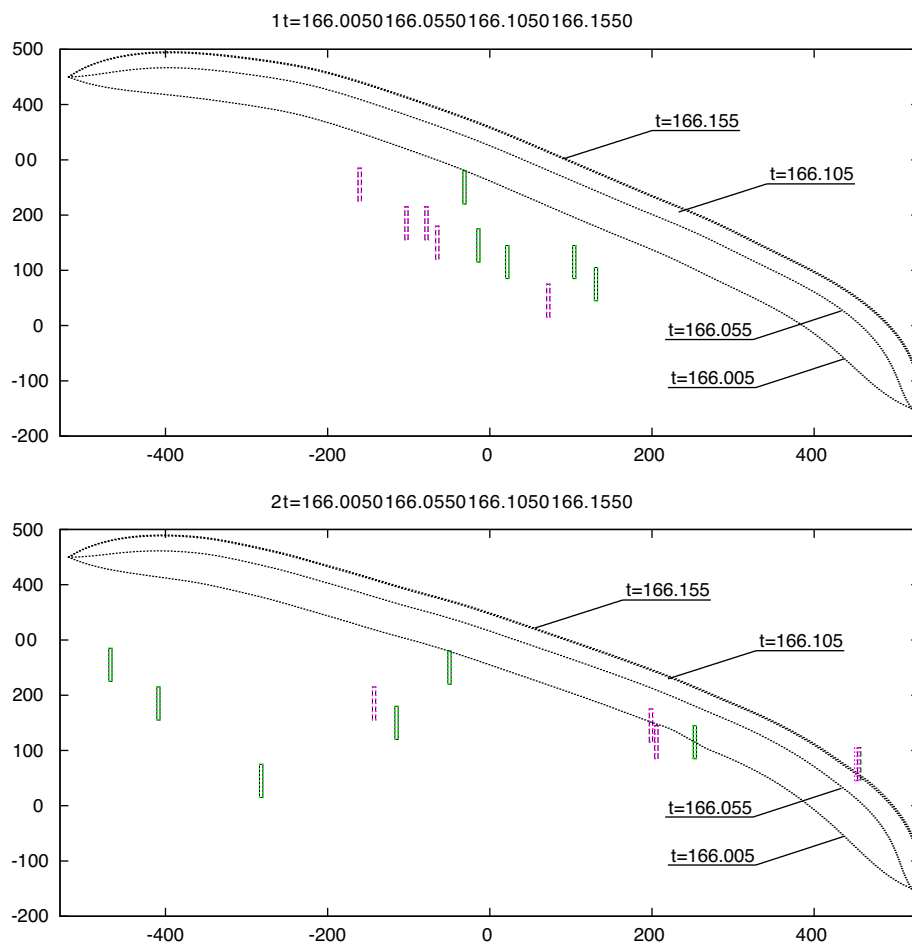


FIG. 3.3. Simulations TEST 1 and TEST 2 – clustering phenomenon observed in TEST 1 and a very different case in TEST 2.

#### REFERENCES

- [1] S.B. Angenent and M.E. Gurtin. Multiphase thermomechanics with an interfacial structure 2. evolution of an isothermal interface. *Arch. Rat. Mech. Anal.*, 108:323–391, 1989.
- [2] G. Dziuk. Convergence of a semi discrete scheme for the curve shortening flow. *Mathematical Models and Methods in Applied Sciences*, 4:589–606, 1994.
- [3] F. Kroupa. Long-range elastic field of semi-infinite dislocation dipole and of dislocation jog. *Phys. Stat. Sol.*, 9:27–32, 1965.
- [4] K. Mikula and D. Ševčovič. Evolution of plane curves driven by a nonlinear function of curvature and anisotropy. *SIAM J. Appl. Math.*, 61(5):1473–1501, 2001.
- [5] V. Minárik and J. Kratochvíl. Dislocation dynamics - analytical description of the interaction force between dipolar loops. *Kybernetika*, 43(6):841–854, 2007.
- [6] V. Minárik, J. Kratochvíl, and K. Mikula. Numerical simulation of dislocation dynamics by means of parametric approach. In M. Beneš, J. Mikyška, and T. Oberhuber, editors, *Proceedings of the Czech Japanese Seminar in Applied Mathematics*, pages 128–138. Faculty of Nuclear Sciences and Physical Engineering, Czech Technical University in Prague, Prague, 2005, ISBN 80-01-03181-0.
- [7] V. Minárik, J. Kratochvíl, K. Mikula, and M. Beneš. Numerical simulation of dislocation dynamics. In M. Feistauer, V. Dolejší, P. Knobloch, and K. Najzar, editors, *Numerical Mathematics*

*and Advanced Applications, ENUMATH 2003 (peer reviewed proceedings)*, pages 631–641. Springer Verlag, 2004, ISBN 3-540-21460-7.

- [8] B. Tippelt, J. Bretschneider, and P. Hähner. The dislocation microstructure of cyclically deformed nickel single crystals at different temperatures. *Phys. Stat. Sol. (A)*, 163:11–26, 1997.